Systems/Circuits

Dendritic Inhibition Provided by Interneuron-Specific Cells Controls the Firing Rate and Timing of the Hippocampal Feedback Inhibitory Circuitry

Leonid Tyan,[1]* Simon Chamberland,[1]* Elise Magnin,[1] Olivier Camiré,[1] Ruggiero Francavilla,[1] Linda Suzanne David,[1] Karl Deisseroth,[2] and Lisa Topolnik[1]

[1]Axis of Cellular and Molecular Neuroscience, Institut Universitaire en Santé Mentale de Québec, Department of Biochemistry, Microbiology and Bio-informatics, Université Laval, Québec G1J 2G3, Canada, and [2]Department of Bioengineering, Stanford University, Stanford, California 94305-5444

In cortical networks, different types of inhibitory interneurons control the activity of glutamatergic principal cells and GABAergic interneurons. Principal neurons represent the major postsynaptic target of most interneurons; however, a population of interneurons that is dedicated to the selective innervation of GABAergic cells exists in the CA1 area of the hippocampus. The physiological properties of these cells and their functional relevance for network computations remain unknown. Here, we used a combination of dual simultaneous patch-clamp recordings and targeted optogenetic stimulation in acute mouse hippocampal slices to examine how one class of interneuron-specific (IS) cells controls the activity of its GABAergic targets. We found that type 3 IS (IS3) cells that coexpress the vasoactive intestinal polypeptide (VIP) and calretinin contact several distinct types of interneurons within the hippocampal CA1 stratum oriens/alveus (O/A), with preferential innervation of oriens-lacunosum moleculare cells (OLMs) through dendritic synapses. In contrast, VIP-positive basket cells provided perisomatic inhibition to CA1 pyramidal neurons with the asynchronous GABA release and were not connected with O/A interneurons. Furthermore, unitary IPSCs recorded at IS3–OLM synapses had a small amplitude and low release probability but summated efficiently during high-frequency firing of IS3 interneurons. Moreover, the synchronous generation of a single spike in several IS cells that converged onto a single OLM controlled the firing rate and timing of OLM interneurons. Therefore, dendritic inhibition originating from IS cells is needed for the flexible activity-dependent recruitment of OLM interneurons for feedback inhibition.

Key words: **dendrite; hippocampus; inhibition; interneuron; optogenetics; paired recording**

Introduction

The hippocampus is a critical region of the medial temporal lobes that supports the ability to recollect consciously and report on facts and events experienced previously (Milner, 1972). This is accomplished through the concerted rhythmic activity of hippocampal networks composed of highly diverse neuronal populations. In particular, the hippocampus contains a large diversity of local-circuit inhibitory interneurons (Klausberger and Somogyi, 2008). These cells have different morphological shapes, express distinct molecular markers, and, importantly, play highly specific roles. Some interneuron subtypes provide perisomatic inhibition to pyramidal cells (PCs), whereas others innervate different dendritic domains of PCs. Therefore, interneurons are ideally positioned to control all stages of the information processing performed by PCs, from input integration to output generation and synchronization of network activity. However, the most striking feature of hippocampal interneurons is their cell-type-specific and activity-dependent recruitment during the hippocampal oscillations that are associated with different behavioral states (Klausberger et al., 2003, 2004, 2005; Nitz and McNaughton, 2004; Lapray et al., 2012). Therefore, the firing rate and timing of interneurons fluctuate continuously in a phase-dependent manner. The mechanisms that control this cell-type-specific and activity-dependent recruitment of interneurons during different brain states are largely unknown.

The fluctuations in interneuron activity may be explained by changes in the excitatory drive that is likely received by interneurons during different phases of network oscillations (Klausberger et al., 2003; Maurer et al., 2006; Tukker et al., 2007; Varga et al., 2012; Pangalos et al., 2013). Alternatively, specific inhibitory mechanisms may exist that coordinate the activity of interneurons tightly (Chamberland and Topolnik, 2012). Intriguingly, a specific population of interneurons that innervate GABAergic cells selectively has been discovered in the hippocampus

Received Sept. 5, 2013; revised Jan. 26, 2014; accepted Feb. 22, 2014.

Author contributions: L. Topolnik designed research; L. Tyan, S.C., E.M., O.C., R.F., L.D., and L. Topolnik performed research; K.D. contributed unpublished reagents/analytic tools; L. Tyan, E.M., O.C., R.F., L.D., and L. Topolnik analyzed data; L. Tyan, O.C., and L. Topolnik wrote the paper.

This work was supported by the Canadian Institutes of Health Research, the Natural Sciences and Engineering Research Council of Canada (NSERC Discovery Grant), and the Savoy Foundation. L.T. is the recipient of a University Faculty Award from NSERC. S.C. and O.C. were supported by doctoral fellowships from NSERC. We thank Dr. Peter Somogyi for stimulating discussions; Charleen Salesse, Magali Grob, and Dimitry Topolnik for excellent technical assistance; and Christopher Lacharité-Mueller for assistance and participation in some of the experiments.

The authors declare no competing financial interests.

Correspondence should be addressed to Lisa Topolnik, Axis of Cellular and Molecular Neuroscience, 2601 Ch. De La Canardière, CRULRG, Québec, PQ, G1J 2G3, Canada. E-mail: Lisa.Topolnik@crulrg.ulaval.ca.

*L.T. and S.C. contributed equally to this work.

DOI:10.1523/JNEUROSCI.3813-13.2014

 0270-6474/14/344534-14$15.00/0

(Acsády et al., 1996a, 1996b; Gulyás et al., 1996). The so-called interneuron-specific (IS) cells were identified based on direct ultrastructural evidence that some calretinin (CR)-expressing or vasoactive intestinal polypeptide (VIP)-expressing GABAergic cells in the CA1 area of the hippocampus contact interneurons selectively. IS cells were further subdivided into three subtypes with distinct anatomical and neurochemical features. However, the physiological properties, targets, and functional significance of IS cells remain unknown. Here, we focused on the type III IS cells (IS3). The somas of these cells are located in the stratum pyramidale (PYR) or radiatum (RAD) and send their axons to the oriens-alveus (O/A) to contact other interneurons located in this area, preferentially metabotropic glutamate receptor 1a (mGluR1a)-positive oriens-lacunosum moleculare interneurons (OLMs) (Acsády et al., 1996b; Chamberland et al., 2010). Accordingly, IS3 cells may play a major role in the regulation of the distal dendritic inhibition of PCs. Using a combination of anatomical analysis, dual simultaneous patch-clamp recordings, and targeted optogenetic stimulation in acute slices obtained from VIP-eGFP and CR-Cre mice, we found that, in addition to OLMs, IS3 cells targeted different classes of CA1 O/A interneurons, including bistratified cells and oriens–oriens interneurons. Although the efficacy of transmission at IS3 synapses was relatively weak, the synchronous activation of many IS3 cells converging onto a single postsynaptic cell controlled its firing rate and timing.

Materials and Methods

Slice preparation. All procedures involving animals were performed in accordance with the animal welfare guidelines of the Animal Protection Committee of Université Laval. Transverse hippocampal slices (thickness, 300 μm) were prepared from VIP/enhanced green fluorescent protein (VIP-eGFP) mice [MMRRC strain #31009, STOCK Tg(Vip-EGFP) 37Gsat, University of California, Davis, CA], or B6(Cg)-Calb2$^{tm1(cre)Zjh/J}$ mice (The Jackson Laboratories) of either sex at postnatal day 19 (P19) to P135. Animals were anesthetized deeply with isoflurane and decapitated. The brain was dissected carefully and transferred rapidly into an ice-cold (0 to +4°C) solution containing the following (in mM): 250 sucrose, 2 KCl, 1.25 NaH_2PO_4, 26 $NaHCO_3$, 7 $MgSO_4$, 0.5 $CaCl_2$, and 10 glucose oxygenated continuously with 95% O_2 and 5% CO_2, pH 7.4, 330–340 mOsm. Slices were cut using a vibratome (VT1000S; Leica Microsystems or Microm; Fisher Scientific), transferred to a heated (35°C) oxygenated recovery solution containing the following (in mM): 124 NaCl, 2.5 KCl, 1.25 NaH_2PO_4, 26 $NaHCO_3$, 3 $MgSO_4$, 1 $CaCl_2$, and 10 glucose; pH 7.4; 300 mOsm and allowed to recover for 1 h. Subsequently, they were kept at room temperature until use.

Patch-clamp electrophysiology. For electrophysiological recordings, slices were transferred to a recording chamber that was perfused continuously (2 ml/min) with normal artificial CSF (ACSF) containing the following (in mM): 124 NaCl, 2.5 KCl, 1.25 NaH_2PO_4, 26 $NaHCO_3$, 2 $MgSO_4$, 2$CaCl_2$, and 10 glucose, pH 7.4 saturated with 95% O_2 and 5% CO_2 at near-physiological temperature (32 ± 1°C). Hippocampal CA1 interneurons were identified visually using an upright fluorescence microscope (Axioscope; Zeiss or TCS SP5; Leica) equipped with a 40× water-immersion objective (numerical aperture [NA] 0.8) and infrared differential interference contrast. Interneurons expressing eGFP in slices from VIP-eGFP mice were identified using blue light (filter set: 450–490 nm). Two-photon images of eGFP-expressing interneurons in acute slices were obtained using a two-photon laser scanning system (TCS SP5; Leica) based on a Ti-Sapphire laser tuned to 900 nm. Images were acquired with a 25× water-immersion objective (NA 0.95; Leica Microsystems). Interneurons expressing mCherry were identified using green light (filter set: 515–560 nm). Recording pipettes (3.5–6 MΩ) were pulled from borosilicate glass capillaries (1B100F-4; World Precision Instruments) using a Flaming/Brown micropipette puller (Sutter Instrument). Whole-cell patch-clamp recordings were obtained from single cells, pairs of interneurons, or pairs of interneurons and PCs. For recordings in current-clamp mode, the intracellular solution contained the following (in mM): 130 $KMeSO_4$, 2 $MgCl_2$, 10 diNa-phosphocreatine, 10 HEPES, 2 ATP-Tris, 0.2 GTP-Tris and 0.3% biocytin (Sigma), pH 7.2–7.3, 280–290 mOsm/L. For recordings performed in voltage-clamp mode, the intracellular solution contained the following (in mM): 130 $CsMeSO_4$, 2CsCl, 10 diNa-phosphocreatine, 10 HEPES, 2 ATP-Tris, 0.2 GTP-Tris, 0.3% biocytin, 2 QX-314, pH 7.2–7.3, 280–290 mOsm/L. Data acquisition (filtered at 2–3 kHz and digitized at 10 kHz) was performed using a Multiclamp 700B amplifier and the Clampex 10.2 software (Molecular Devices).

Passive membrane properties (resting membrane potential, input resistance, and membrane capacitance) were obtained immediately after membrane rupture. Membrane capacitance was determined using the square pulse (5 mV, 10 ms) method of the membrane test in Clampex 10.2 software (Gillis, 1995). Active membrane properties were recorded in current-clamp mode by subjecting cells to multiple current step injections of varying amplitudes (−200 to 280 pA). The ratio of the last and first interspike interval and the maximal firing frequency were determined at 280 pA. To assess synaptic connectivity, two neurons were recorded simultaneously, with the presynaptic interneuron kept in current-clamp mode at −60 mV and the postsynaptic cell held in voltage-clamp mode at 0 mV. The junction potential was not corrected. Action potentials (APs) were evoked in the presynaptic interneuron via 2 brief somatic current injections (2 ms, 0.5–1.5 nA) at 20 Hz. In the case of synaptic connection, this protocol evoked short-latency (<5 ms) unitary IPSCs (uIPSCs) in the postsynaptic cell. For variance–mean (*V–M*) analysis, uIPSCs were recorded in ACSF containing different concentrations of Ca^{2+} and Mg^{2+}: 3.8 mM Ca^{2+} and 0.2 mM Mg^{2+}; 2.0 mM Ca^{2+} and 2.0 mM Mg^{2+}; or 1 mM Ca^{2+} and 3 mM Mg^{2+}. The concentration of Mg was adjusted to keep the concentration of bivalent ions constant. The pipette capacitance and series resistance (in voltage-clamp configuration) were compensated and bridge balance (in current-clamp configuration) was adjusted. The access resistance (R_a) was monitored continuously by applying a −5 mV step at the end of every sweep. Recordings with changes in R_a >15% were discontinued. In some experiments, gabazine (1 μM; Abcam) or bicuculline (10 μM; Sigma) were applied to confirm the $GABA_A$ nature of the synaptic currents. The ionotropic glutamate receptor antagonists L-AP5 (100 μM) and NBQX (10 μM) (both from Abcam) and the sodium-channel blocker tetrodotoxin (TTX; 1 μM; Alomone Laboratories) were applied in some experiments.

Optogenetic targeting of interneurons. Expression of channelrhodopsin 2 (ChR2) in CR-positive interneurons was achieved using a Cre-loxP approach. Heterozygous or homozygous B6(Cg)-Calb2$^{tm1(cre)Zjh/J}$ mice (P21–P29) were anesthetized deeply via the intraperitoneal injection of ketamine/xylazine (0.1 ml/10 g). Animals were placed in a stereotaxic frame (Kopf Instruments) and bilateral craniotomies were performed according to the following bregma coordinates: A–P, +2.4 mm; M–L, ±2.4 mm; and D–V, −1.3 mm. The injection pipette, which was attached to a microprocessor-controlled nanoliter injector (Nanoliter 2000; World Precision Instruments), was slowly lowered into the hippocampus at a speed of 1 mm/min. Hippocampal injections of the adeno-associated virus rAAV5-EF1a-DIO-hChR2(H134R)-mCherry-WPRE-pA (4×10^{12} virus molecules/ml; Vector Core Facility, University of North Carolina) were performed bilaterally. A total volume of 1.0–1.2 μl/hemisphere was administered in 2 applications with a 2 min interval at a rate of 5 nL/s. Two minutes after the final injection, the pipette was slowly withdrawn, the scalp was sutured, and the animals were given an analgesic (Anafen, 0.04–0.1 ml/10 g) and allowed to recover. Three to 6 weeks after the injections, the animals were killed and acute hippocampal slices were prepared.

Light stimulation of single ChR2-expressing interneurons was achieved by scanning the cell body (diameter of the region of interest, 10–15 μm) of mCherry-expressing cells with a 488 nm argon laser (Leica Microsystems) for 22 ms. A 40× water-immersion objective (NA 0.8) was used in these experiments. Light-evoked IPSCs ($IPSC_L$s) were recorded at 0 mV. Pairs of interneurons were considered to be connected when laser stimulation of the mCherry-expressing interneuron evoked $IPSC_L$s in the postsynaptic cell. In this case, the laser intensity was

Table 1. Membrane and neurochemical properties of IS-3 versus BC

	BC	IS3
Resting membrane potential (mV)	−63.55 ± 1.6* ($n = 10$)	−74.2 ± 0.7 ($n = 9$)
Input resistance (MΩ)	251.4 ± 50.1*** ($n = 10$)	496.9 ± 28.6 ($n = 46$)
Membrane capacitance (pF)	49.7 ± 4.7* ($n = 10$)	38.5 ± 2 ($n = 45$)
Rheobase (pA)	70 ± 11.3 ($n = 6$)	42.8 ± 8 ($n = 23$)
AP threshold (mV)	−43.25 ± 2.4 ($n = 6$)	−44.6 ± 1.4 ($n = 23$)
AP amplitude (mV)	80.4 ± 6.1 ($n = 6$)	86.3 ± 2.2 ($n = 23$)
AP duration (ms)	1.02 ± 0.05 ($n = 6$)	1.1 ± 0.06 ($n = 23$)
Ratio of the last and first interspike intervals	4.05 ± 0.4 ($n = 6$)	3.16 ± 0.9 ($n = 8$)
Maximal firing frequency (Hz)	156 ± 17 ($n = 6$)	171 ± 17 ($n = 8$)
Calretinin	−	+
Somatostatin	−	−
Muscarinic receptor 2	NT	−
Cholecystokinin	+	−
Neuropeptide Y	−	−

NT, Not tested.

*$p < 0.05$; **$p < 0.01$; ***$p < 0.001$.

Table 2. Target-specific properties of uIPSCs

	OLM ($n = 18$)	BIS ($n = 5$)	OO ($n = 6$)
Failure rate (%)	59.7 ± 6.0	59.2 ± 9.8	58.2 ± 10.6
uIPSC potency (pA)	18.1 ± 4.5	21.7 ± 3.4	10.9 ± 2.3##
Inhibitory conductance (nS)	0.25 ± 0.06	0.3 ± 0.05	0.15 ± 0.03##
Rise time (ms)	1.3 ± 0.1	0.73 ± 0.06*	1.1 ± 0.2#
Decay τ (ms)	9.0 ± 0.7	5.1 ± 0.5**	10.2 ± 1.9#
Latency (ms)	1.9 ± 0.2	1.7 ± 0.3	1.7 ± 0.1
Coefficient of variation	0.35 ± 0.01	0.34 ± 0.03	0.4 ± 0.08
PPR failures included	1.1 ± 0.09	1.2 ± 0.3	1.2 ± 0.3

OO, oriens– oriens interneuron.

*$p < 0.05$; **$p < 0.01$ compared with OLM.

#$p < 0.05$; ##$p < 0.01$ compared with BIS.

brought to the minimal, resulting in some failures and some successful $IPSC_L$s.

Synchronous activation of several IS3 cells (and their axons) was achieved using wide-field stimulation with blue light for 5 ms via a 40× water-immersion objective (NA 0.8; Axioscope, filter set, 450–490 nm; Zeiss) that was controlled by an ultrafast shutter (Uniblitz Electronic). For recordings of $IPSC_L$s, a high-chloride (50 mM) intracellular solution was used and cells were held at −70 mV. In the experiments illustrated in Figure 8, current-clamp recordings were obtained from OLM interneurons (which were confirmed anatomically *post hoc*) that were depolarized to ~−45 mV by current injection for 2 s to allow spontaneous firing. The IPSPs evoked by light ($IPSP_L$s) and the associated changes in the AP probability were analyzed.

Data analysis. Analysis of electrophysiological recordings was performed using Clampfit 10.2 (Molecular Devices) and Igor Pro 6.2 (WaveMetrics). AP properties were derived from the first AP that occurred within the 50 ms time window from the beginning of the current pulse (+50 to 100 pA). The AP threshold was determined using the first maximal derivative (dV/dt) of the voltage trace recorded. The AP amplitude was measured from the baseline (Table 1) or from the threshold level (see Fig. 7*A*). The AP latency was determined as the time interval from the beginning of the current pulse to the threshold of the AP. The AP duration was measured as the half-width time of the AP.

To analyze the properties of uIPSCs, 100 sweeps were acquired. Sweeps that were contaminated by spontaneous activity occurring right before or during uIPSCs were removed. The remaining sweeps were inspected visually and the failure rate was calculated as the number of failures divided by the total number of noncontaminated traces. After this step, all sweeps containing failures were removed and successful uIPSCs (minimum of 20 sweeps) were averaged for further analysis. The uIPSC latency was determined as the time interval between the peak of an AP that was initiated in the presynaptic cell and the onset of the uIPSC in the postsynaptic cell. uIPSC potency was measured as the peak uIPSC amplitude excluding failures. The rise time of uIPSC was taken at 20–80%. The decay τ of the uIPSC was fitted with a single exponential. The synaptic conductance was determined using the following equation:

$$I = G \times (V_{hold} - V_{rev}) \quad (1)$$

where I is the peak current amplitude (pA), G is the synaptic conductance (nS), V_{hold} is the holding potential (mV), and V_{rev} is the IPSC reversal potential (mV) determined experimentally in OLMs using the same intracellular solution (−71.9 ± 1.2 mV; Salesse et al., 2011).

The coefficient of variation (CV) was measured as the SD of the uIPSC amplitude divided by the mean, including failures. The paired-pulse ratio was determined as the ratio between the mean peak amplitude of the second response and the mean peak amplitude of the first response, which were obtained 50 ms apart, including failures. During repetitive stimulation (10–100 Hz), the peak amplitudes of individual uIPSCs (see Fig. 4*D*) or the peak amplitude of the total inhibitory current (see Fig. 4*E*) were measured.

For *V–M* analysis, 100 sweeps were acquired for each release probability condition ($[Ca^{2+}]_i$ = 1.0, 2.0, and 3.8 mM). Traces contaminated by spontaneous activity occurring right before or during uIPSCs were removed and the means and variances of uIPSC amplitude were analyzed. The baseline noise variance was subtracted from the variance obtained in each condition. The relationship between variance (δ^2) and mean (x) was fit with the linear equation (Clements and Silver, 2000; Lawrence et al., 2004) using Igor Pro software as follows:

$$\delta^2 = (1 + CV^2) \times qx \quad (2)$$

where q is the quantal amplitude. Based on our own observations for uIPSC properties at IS3–OLM synapses (Table 2), we fixed the CV at 0.35. In one case, a binomial approximation was used to determine the *V–M* relationship in Clampfit 10.2 as follows:

$$\delta^2 = (1 + CV^2) \times qx - x^2/n \quad (3)$$

For the analysis of spike probability in optogenetic experiments, seven individual APs were averaged to create the AP search template in Clampfit 10.2, which was then used to count all APs recorded during light stimulation. The spike probability was determined as the average number of spikes per trace that occurred within a 300–2000 ms window (Fig. 8).

All data are presented as means ± SEM. Statistical significance was evaluated with Student's paired or unpaired t test, the Mann–Whitney test, or ANOVA (*$p < 0.05$, **$p < 0.01$, ***$p < 0.001$).

Morphological and neurochemical analyses. For *post hoc* anatomical reconstruction, all recorded neurons were filled with biocytin (Sigma) during whole-cell recordings. Slices with recorded cells were fixed overnight with 4% paraformaldehyde at 4°C and then kept in PB (0.1 mM). To reveal biocytin, the 300 μm slices were treated with H_2O_2 (0.3%) for 30 min, permeabilized with 1.5% Triton X-100 in TBS for 0.5–1.0 h, and blocked with 10% NGS and 0.5% BSA in TBS for 0.5–1.0 h. Finally, slices were incubated with streptavidin-conjugated Alexa Fluor 546 (1:200) or streptavidin-conjugated Alexa Fluor 488 (1:200) overnight at 4°C. The following day, slices were rinsed and mounted on a microscope slide with Dako Fluorescent Mounting Medium. Confocal images of biocytin-filled interneurons were obtained using a Leica TCS SP5 imaging system coupled to a 488 nm argon or a 543 nm HeNe lasers. *Z*-stacks were acquired using a 20× (NA 0.8) or a 63× (NA 1.4) oil-immersion objective (Leica Microsystems). Anatomical reconstruction was performed using Neurolucida 8.26.2 software (MBF Bioscience).

For immunohistochemical analysis of molecular markers expressed by interneurons, animals were perfused with 4% paraformaldehyde and hippocampal sections (thickness, 50–70 μm) were prepared using a vibratome (VT1000; Leica Microsystems). Sections were permeabilized with 0.2–0.3% Triton X-100 in TBS and incubated in blocking solution containing 4% BSA and 10–20% normal serum for 1 h. After this step, sections were incubated with primary antibodies at 4°C for 24–48 h. The following day, slices were incubated with conjugated secondary antibod-

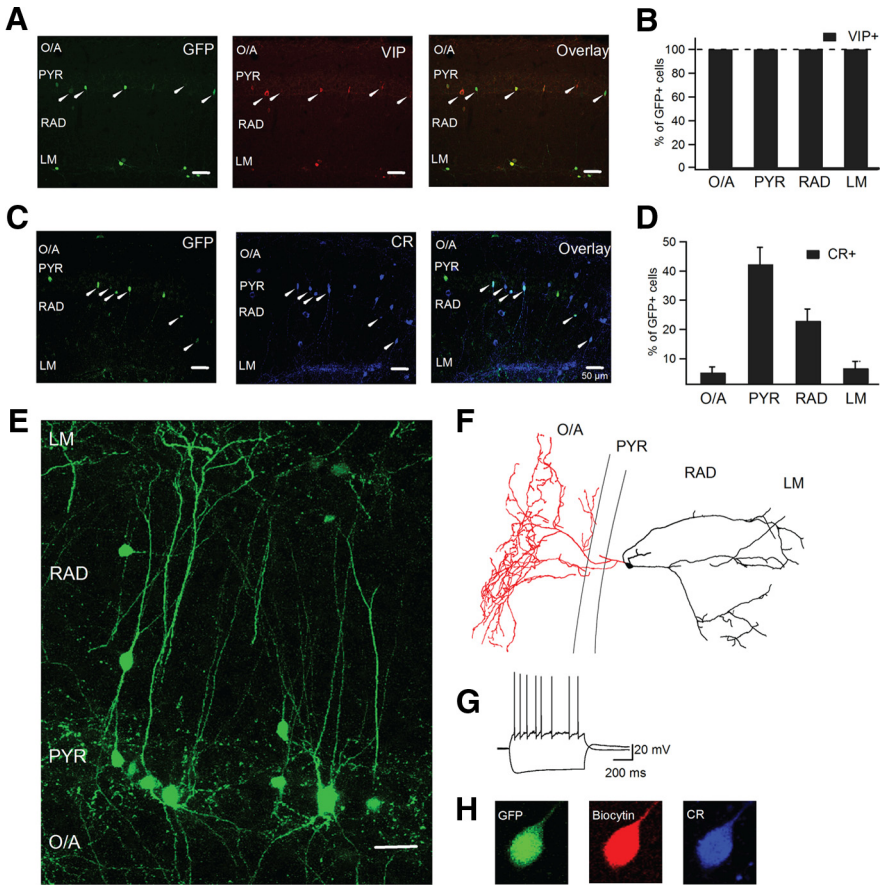

Figure 1. Identification of IS3 cells in the VIP-eGFP mouse model. ***A***, Confocal images showing immunoreactivity for GFP (left), VIP (middle), and a superimposition of the two markers (right). ***B***, Summary bar graphs illustrating the degree of colocalization between VIP and GFP in different layers of the hippocampal CA1 area of the VIP-eGFP mouse ($n = 15$ slices/three animals). ***C***, Confocal images showing immunoreactivity for GFP (left), CR (middle), and a superimposition of the two markers (right). ***D***, Summary data illustrating the colocalization of CR and GFP in different layers of the hippocampal CA1 area of the VIP-eGFP mouse ($n = 10$ slices/two animals). Scale bars, 50 μm. ***E***, Two-photon image (maximal projection of a *z*-stack) of the CA1 area from an acute hippocampal slice (300 μm) of a VIP-eGFP mouse showing the morphological features of VIP-positive interneurons in the CA1 area. Scale bar, 20 μm. ***F***, Anatomical reconstruction (the axon is shown in red, the dendrites are shown in black) of an IS3 cell that was recorded and filled with biocytin in slices obtained from VIP-eGFP. ***G***, Representative voltage responses of an IS3 interneuron to positive (+50 pA) and negative (−100 pA) current injections. ***H***, Confocal images showing CR expression by IS3 interneurons.

ies (FITC, Alexa Fluor 488, Cy3, or DyLight-647; Jackson ImmunoResearch) for 2–4 h, rinsed, and mounted on microscope slides. Confocal images of labeled sections were obtained using a Leica TCS SP5 imaging system equipped with a 488 nm argon, a 543 nm HeNe, or a 633 nm HeNe laser and a 20× (NA 0.8) or a 63× (NA 1.4) oil-immersion objective (Leica Microsystems). Cells expressing specific markers (Figs. 1, 6*A*) were counted in different CA1 layers. The cells were considered immunopositive when the corresponding fluorescence intensity was at least twice that of the background. For representation only, the overall brightness and contrast of images were adjusted manually. Portions of images were not modified separately in any way.

The combined anatomical, neurochemical, and electrophysiological identification of interneurons was obtained by recording the membrane properties of cells in current-clamp mode for 5 min and filling interneurons with biocytin. Slices with recorded cells were then fixed, embedded in 4% agar, and resectioned to 50 μm sections. Sections were processed for biocytin and tested for the expression of different markers. The following primary antibodies were used in this study: rabbit anti-VIP (catalog #9535-0204, 1:1000; AbD Serotec,), rabbit anti-VIP (catalog #20077, 1:400; Immunostar), goat anti-CR (catalog #sc-11644, 1:1000; Santa Cruz Biotechnology), rabbit anti-cholecystokinin 26–33 (CCK-8) (1:200; Sigma, #C2581), sheep anti-neuropeptide Y (NPY; catalog #AB1583, 1:500; Millipore), rabbit anti-muscarinic receptor 2 (M2R; catalog #HPA029795, 1:200; Sigma), rabbit anti-SOM (catalog #ab64053, 1:500; Abcam), rabbit anti-mCherry (catalog #5993-100, 1:500; BioVision), mouse anti-GFP (catalog #ab1218, 1:200; Abcam), and chicken anti-GFP (catalog #GFP-1020, 1:1000; Aves).

Results

Properties and connectivity of IS3 interneurons

To target IS3 cells selectively, we combined single and dual patch-clamp recordings with detailed anatomical and neurochemical analyses and optogenetic manipulations in hippocampal slices obtained from two types of transgenic mice: VIP-eGFP and CR-Cre. Given that IS3 cells express VIP, initially we used a VIG-eGFP mouse model for targeted patch-clamp recordings from VIP-expressing interneurons in the CA1 region of the hippocampus. In this mouse model, virtually all GFP-expressing CA1 interneurons were positive for VIP ($n = 398/398$ cells/three animals; Fig. 1*A*,*B*), which rendered it suitable for studying hippocampal VIP-positive cells. According to previous reports, IS3 cells in the rat hippocampus represent a subpopulation of VIP-expressing interneurons that are positive for CR (Acsády et al., 1996a, 1996b; Gulyás et al., 1996). These cells are mainly located within the stratum pyramidale (PYR) and the stratum radiatum (RAD) (Acsády et al., 1996a, 1996b; Ferraguti et al., 2004; Chamberland et al., 2010). Consistent with these observations, we found a large proportion of GFP-positive cells within PYR and RAD that coexpressed CR (42.3 ± 5.8% and 22.9 ± 4.1%, respectively; $n = 10$ slices/two animals; Fig. 1*C*,*D*), thereby corresponding to the IS3 interneurons. A subpopulation of GFP-expressing interneurons was also found within the stratum lacunosum-moleculare (LM; Fig. 1*A*). These cells were CR-negative and could correspond to the type 2 IS interneurons described previously in the rat CA1 hippocampus (Acsády et al., 1996a, 1996b).

Next, we assessed the properties of IS3 cells by performing targeted patch-clamp recordings followed by anatomical and neurochemical analyses of recorded interneurons. Previous studies showed that IS3 cells have a bipolar orientation, with dendrites spanning all CA1 layers and branching extensively within the LM and the axon projecting to the O/A (Acsády et al., 1996a, 1996b). In fact, GFP-expressing cells with such morphological features were found routinely in the CA1 area of the hippocampus (Fig. 1*E*). We filled these cells with biocytin during whole-cell patch-clamp recordings to perform detailed anatomical reconstructions (Fig. 1*F*). IS3 cells exhibited unipolarly or bipolarly oriented dendritic arbors (Fig. 1*F*) and had an axon that occupied mainly the O/A (95.3 ± 1.2%; $n = 6$) and branched occasionally within the RAD and PYR (4.7 ± 1.2%; $n = 6$). The total number of axonal boutons within the O/A, as

estimated from the completely reconstructed IS3 cells, varied from 47 to 89 (n = 6 cells). Consistent with previous reports (Chamberland et al., 2010, Tricoire et al., 2010), these cells had a high input resistance (496.9 ± 28.6 MΩ; n = 46; Table 1), small membrane capacitance (38.5 ± 2.0 pF; n = 45; Table 1), and exhibited an irregularly spiking firing pattern (Fig. 1*G*), although regularly spiking adapting firing was also observed (n = 3/23 cells). To obtain the molecular profile of IS3 cells, we performed short-duration whole-cell recordings (5 min after cell rupture) to prevent the extensive washout of intracellular compounds, which was followed by a *post hoc* neurochemical analysis. These data showed that IS3 cells were negative for SOM, CCK, NPY, and M2R, but expressed CR (Fig. 1*H*).

To study the postsynaptic targets of IS3 cells, next we examined their connectivity with CA1 O/A interneurons and PCs. Previous studies have reported that IS3 cells prefer to make synapses onto mGluR1α-expressing O/A interneurons, although CB-positive interneurons were also contacted by these cells (Acsády et al., 1996b; Gulyás et al., 1996). To determine the anatomical identity of IS3 postsynaptic targets and the properties of IS3 synapses, we performed paired recordings from PYR/RAD GFP-positive cells and O/A interneurons in slices obtained from VIP-eGFP mice. In total, among the 160 pairs tested, 54 pairs were connected synaptically. Neurolucida reconsruction (32 of 54 pairs) revealed the morphological identity of the target cells, which included OLMs (n = 18, Fig. 2*A*,*E*), bistratified cells (BISs; n = 5, Fig. 2*B*,*E*), basket cells (BCs; n = 3, Fig. 2*C*,*E*), and horizontally oriented interneurons with extensive branching within the O/A (the so-called oriens–oriens interneurons; n = 6, Fig. 2*D*,*E*). In all cases, IS3 interneurons provided dendritic inhibition to their targets (Fig. 2*A*–*D*). Accordingly, uIPSCs recorded at 0 mV had small amplitude and relatively slow rise time at all targets (uIPSC potency, 18.6 ± 2.9 pA; uIPSC rise time, 1.1 ± 0.1 ms; n = 32; t = 32°C; Table 2). The small amplitude of uIPSCs was not a result of the depolarization-induced suppression of inhibition that could occur at 0 mV (Pitler and Alger, 1992; Vincent et al., 1992) because IPSCs recorded at −70 mV (using a 50 mM $[Cl^-]_i$ intracellular solution) were not affected by the 5 s membrane depolarization to 0 mV (IPSC amplitude control, −28 ± 4.8 pA; IPSC amplitude after depolarization, −28.3 ± 4.3 pA; n = 4). We found significant differences in uIPSC kinetics between BISs and OLMs, with uIPSCs at IS3–BIS synapses having the fastest rise and decay (Table 2). In addition, both the uIPSC potency and kinetics were different between BIS and oriens–oriens cells, resulting in a significantly smaller inhibitory conductance in oriens–oriens interneurons (Table 2). These data point to target-specific dendritic filtering or to the synapse-specific composition of the $GABA_A$ receptor, which will need to be examined further in detail. Furthermore, uIPSCs at all IS3 synapses had a similar failure rate and coefficient of variation and exhibited small paired-pulse facilitation (Fig. 2*A*–*D*; Table 2), suggesting that the properties of GABA release are similar at different IS3 interneuron targets. Finally, we found no evidence of a synaptic connection between IS3 cells and CA1 PCs (n = 11 pairs), which is consistent with previous ultrastructural findings on the preferential innervation of interneurons by IS3 cells (Acsády et al., 1996b; Gulyás et al., 1996).

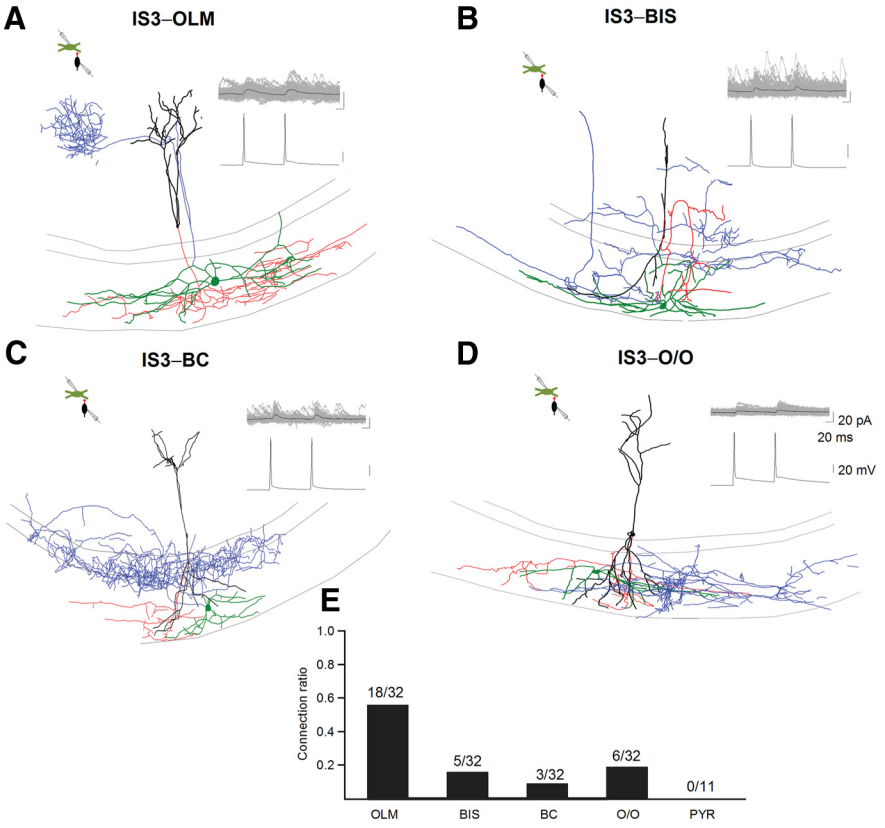

Figure 2. IS3 cells provide dendritic inhibition to different subtypes of CA1 O/A interneurons. ***A–D***, Anatomical reconstructions of synaptically connected pairs of interneurons illustrating the postsynaptic targets of IS3 cells. The axon of a presynaptic IS3 cell is shown in red and its dendrites are shown in black. The axon of the postsynaptic O/A interneuron is shown in blue, with its dendrites shown in green. The insets shown on the right show examples of paired recordings from reconstructed neurons. Upper traces represent voltage-clamp recordings of uIPSCs at 0 mV (100 consecutive traces are shown in gray and the average, including failures, is shown in black). The lower traces are current-clamp recordings of APs evoked by the current injection in a presynaptic IS3 cell. The insets shown in the top left corner illustrate schematically the configuration of the recording. Note that OLMs (n = 18; ***A***), BISs (n = 5; ***B***), BCs (n = 3; ***C***), and oriens–oriens interneurons (n = 6; ***D***) were among the postsynaptic targets of IS3 cells. ***E***, Summary bar graph illustrating the connection ratio for different postsynaptic targets.

Together, our data indicate that IS3 cells provide dendritic inhibition to different subtypes of inhibitory interneurons located within the CA1 O/A. Given that the main excitatory input in this area originates from local CA1 PC collaterals (Blasco-Ibáñez and Freund, 1995; Takács et al., 2012), our data suggest that IS3 cells are well positioned to control mainly the feedback recruitment of O/A interneurons.

VIP-positive basket cells show distinct properties and connectivity

In addition to IS3 interneurons, VIP is expressed by the CCK-positive BCs (Kosaka et al., 1985; Sloviter and Nilaver, 1987; Acsády et al., 1996a, 1996b). Accordingly, VIP-positive BCs were recorded occasionally in our experiments (n = 10 of 53 VIP-positive interneurons identified anatomically). Given the importance of distinguishing the two interneuron types, we analyzed the properties and functional connectivity of VIP-positive BCs. First, we found clear

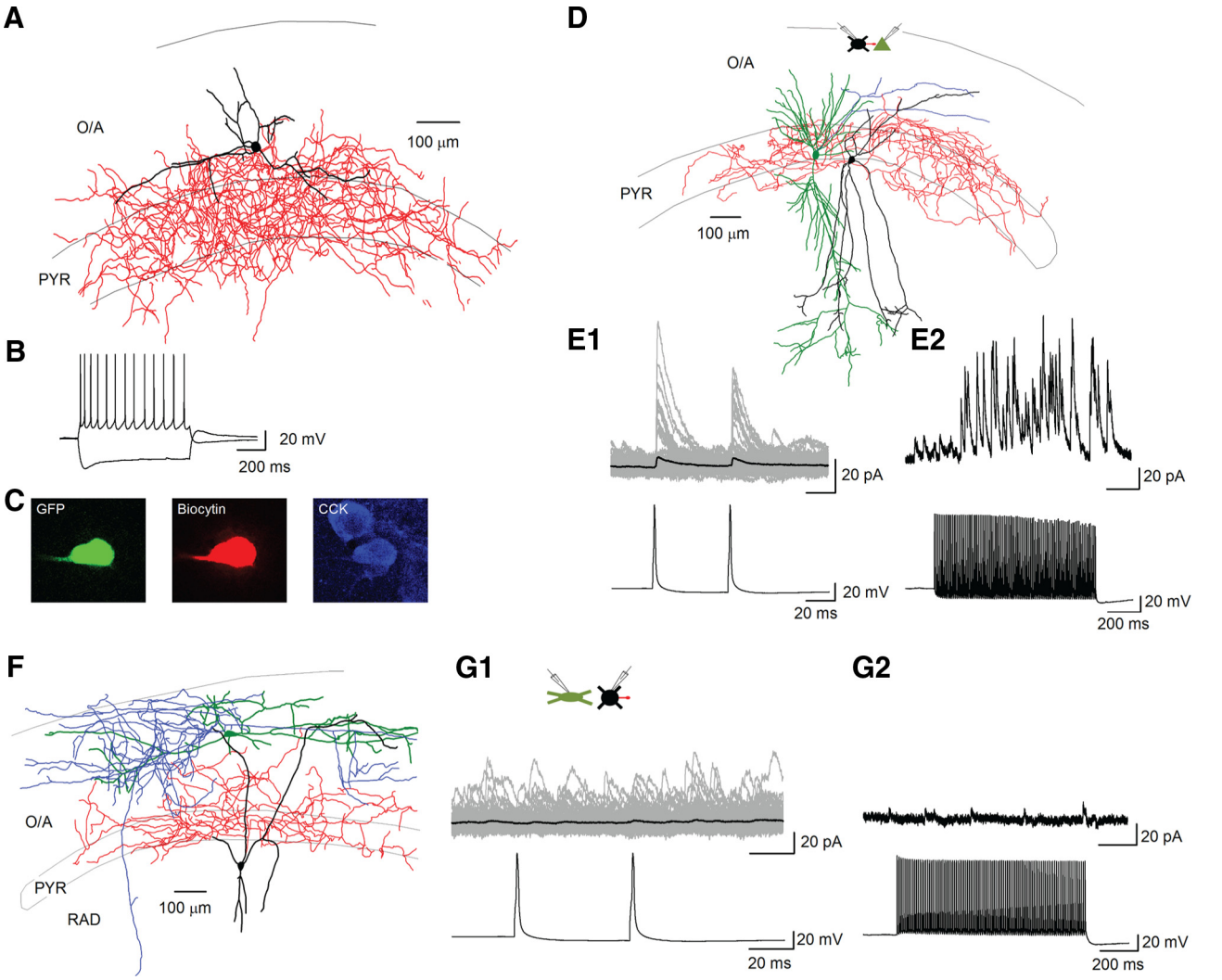

Figure 3. VIP-expressing basket cells provide perisomatic inhibition to CA1 PCs ***A***, Anatomical properties of VIP-positive BCs, as shown by a representative reconstruction, which illustrates the preferential targeting of the PYR layer by this cell type. The axon is shown in red and the dendrites are shown in black. ***B***, Representative voltage responses of a BC to positive (+50 pA) and negative (−100 pA) current injections. ***C***, Confocal images showing immunoreactivity for CCK in VIP-positive BCs. ***D***, Anatomical reconstruction of a synaptically connected VIP-positive BC (the dendrites are shown in black and the axon is shown in red) and PC (the dendrites are shown in green and the axon is shown in blue) pair. The inset shown on top illustrates schematically the configuration of the recording. ***E***, Representative examples of the uIPSCs (V_h = 0 mV; 100 consecutive traces are shown in gray and the average, including failures, is shown in black) evoked in the PC by two APs in the BC (***E1***) and the uIPSCs recorded in the PC during a 100 Hz train of APs in the BC (***E2***). Note the asynchronous release of GABA at VIP-positive BC−PC synapses. ***F***, Anatomical reconstruction of an unconnected VIP-positive BC to an O/A interneuron pair. ***G***, Representative examples of recordings from an unconnected pair (100 consecutive traces are shown in gray and the average, including failures, is shown in black), showing responses to two evoked APs in the presynaptic cell (G1) and to a train of APs in the presynaptic cell (G2).

differences in the axonal arborization of BCs as they targeted mostly PYR and adjacent stratum oriens (PYR: 56%, oriens: 27%, RAD: 17%; Fig. 3*A*,*D*,*F*, respectively). Second, BCs exhibited significantly smaller input resistance (251.4 ± 50.1 MΩ; $n = 10$; $p < 0.001$; *t* test; Table 1), a higher membrane capacitance (49.7 ± 4.7 pF; $n = 10$; $p < 0.05$; *t* test; Table 1), and a mostly regularly spiking firing pattern (Fig. 3*B*). In contrast to IS3 cells, VIP-positive BCs were negative for CR but expressed CCK (Fig. 3*C*). Consistent with previous reports (Heft and Jonas, 2005; Glickfeld and Scanziani, 2006; Daw et al., 2009), VIP-positive BCs provided perisomatic inhibition to PCs (uIPSC potency, 28.2 ± 5.7 pA; rise time, 0.7 ± 0.2 ms; decay time constant, 7.1 ± 1.2 ms; $n = 4$; Fig. 3*D*,*E1*) with asynchronous release (Fig. 3*E2*). Furthermore, we found no evidence of a synaptic connection between VIP-positive BCs and O/A interneurons ($n = 16$ pairs). In conclusion, our results showed that VIP-positive BCs can be clearly distinguished from VIP-positive IS3 cells based on a combination of anatomical, physiological, and neurochemical criteria, as well as on functional connectivity. Furthermore, the properties of VIP-positive BCs examined here were similar to those reported for CCK-positive BCs in previous studies (Hefft and Jonas, 2005; Glickfeld and Scanziani, 2006; Daw et al., 2009; Földy et al., 2010).

Properties of IS3–OLM synapses

It has been suggested that SOM-/mGluR1α-expressing OLM cells represent the major postsynaptic target of IS3 cells (Acsády et al., 1996b). The results of our experiments support this hypothesis. Therefore, we analyzed the properties of transmission at IS3–OLM synapses in greater detail. uIPSCs in OLMs were blocked by the $GABA_A$ receptor antagonists gabazine or bicuculline (decrease to 8.8 ± 3.5% of control, $n = 5$; Fig. 4*A1*), confirming their GABAergic nature. Consistent with the dendritic location of synapses, uIPSCs had an overall small amplitude and slow kinetics (Fig. 4*A*,*B*, Table 2). A large variability in uIPSC potency, rise time, and decay time constant could reflect different

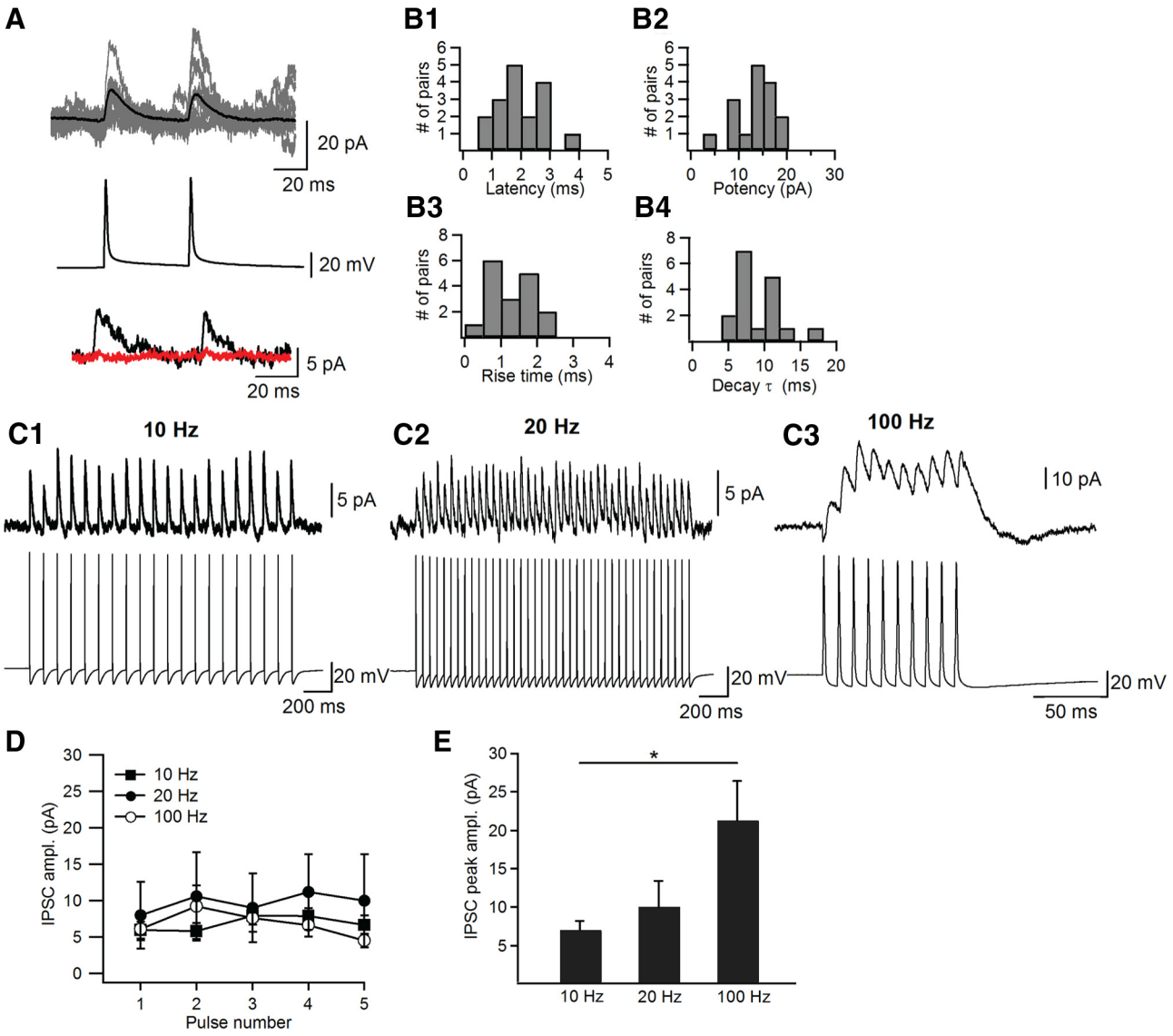

Figure 4. Properties of transmission at IS3–OLM synapses ***A***, Representative examples of uIPSCs evoked in the OLM interneuron by two APs in IS3 (10 consecutive traces are shown in gray and the average, including failures, is shown in black). Bottom traces indicate the effect of gabazine on uIPSCs (the control response is shown in black and the response in presence of gabazine is shown in red). ***B***, Cumulative histograms of uIPSC latency (***B1***), potency (***B2***), rise time (***B3***), and decay time constant (***B4***). ***C***, Representative traces (average of 10 sweeps) illustrating the changes in uIPSC amplitude during different frequencies of firing of an IS3 cell: 10 Hz (***C1***), 20 Hz (***C2***), and 100 Hz (***C3***). ***D***, Summary plot showing changes in uIPSC amplitude during the 10, 20, and 100 Hz firing of an IS3 cell. ***E***, Summary graph illustrating the enhancement in uIPSC peak amplitude during 100 Hz firing of an IS3 cell due to summation of uIPSCs ($n = 6$; $p < 0.05$, paired t test). In ***C–E***, failures were not excluded during the analysis.

numbers of synaptic contacts and their distinct dendritic location resulting in a different degree of electrotonic filtering. Furthermore, the amplitude of individual uIPSCs showed no significant changes during repetitive firing of IS3s (10–100 Hz; $n = 6$; $p > 0.05$; Fig. 4*C*,*D*). However, when an IS3 cell fired at 100 Hz, the peak amplitude of the total inhibitory current increased significantly due to efficient summation of individual uIPSCs ($n = 6$; $p < 0.05$; ANOVA; Fig. 4*C*3,*D*,*E*). These data indicate that dendritic inhibition provided by IS3 cells increases substantially when these cells fire at high frequency.

To estimate the number of release sites and the quantal size at IS3–OLM synapses, we performed a *V–M* analysis of uIPSCs. The amplitude of uIPSCs and their variance were monitored under different release probability conditions by varying the extracellular calcium concentration from 1 to 3.8 mM (Fig. 5*A*,*B*). Consistent with a low release probability at this synapse, both the amplitude of uIPSCs and their variance increased linearly with increasing release probability. The *V–M* plot was fit with a straight line, indicating that release probability remained low even in high calcium concentration ($n = 6/7$ pairs, Fig. 5*C*,*D*). The slope of the *V–M* fit yielded a quantal amplitude of 5.6 ± 0.4 pA. In one pair, the *V–M* relationship was approximated by a parabola, which indicated the quantal size of 5.9 pA with three release sites. It should be pointed out that the actual number of release sites at IS3–OLM synapses could not be determined in our study and will require additional electron microscopic analysis. These data show that a single IS3 cell contacted an OLM cell via synapses with multiple release sites and provided dendritic inhibition with a small quantal size and a low release probability.

Optogenetic targeting of IS3 cells

The small amplitude of uIPSCs at IS3–OLM synapses suggests a small impact on the output of OLM interneurons. However, the dense axonal arborization within the O/A that originates from

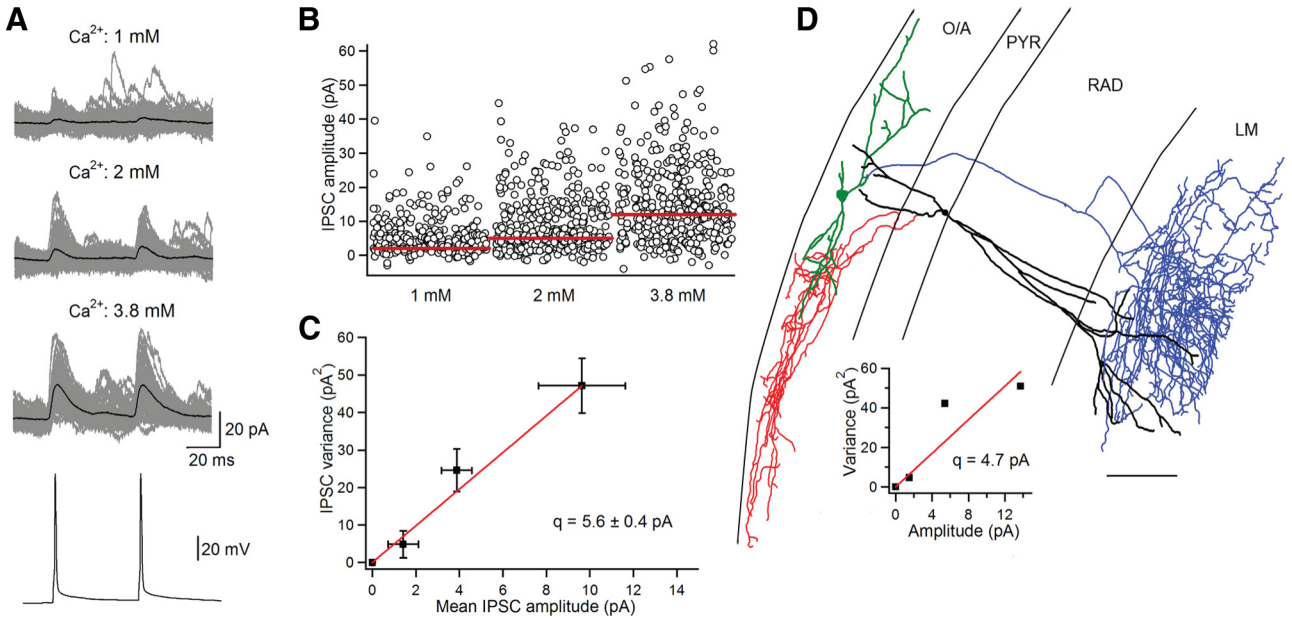

Figure 5. *V–M* analysis of transmission at IS3–OLM synapses. ***A***, Sample traces (gray) and average uIPSC (black) recorded in an OLM interneuron under different release probability conditions (extracellular Ca^{2+} concentration, 1, 2, and 3.8 mM). ***B***, Scatter plot of uIPSC amplitude recorded under the release probability conditions shown in ***A***. ***C***, Summary *V–M* analysis plot showing the quantal size (q) at IS3–OLM synapses ($n = 7$). ***D***, Anatomical reconstruction of the connected pair of IS3 and OLM interneurons from which the recordings shown in ***A*** were obtained. The inset shows the *V–M* analysis plot for this pair of interneurons.

IS3 cells indicates that many IS3 cells are likely to converge onto a single OLM. Furthermore, given the dendritic initiation of the AP in OLM interneurons (Martina et al., 2000), synchronous activation of several IS3 cells during network activity may have a significant impact on OLM output.

To test this hypothesis, we applied a combination of patch-clamp recordings with optogenetic stimulation in slices from CR-Cre mice. Heterozygous (HE) or homozygous (HO) mice were stereotaxically injected with a double-floxed Cre-dependent adeno-associated virus: rAAV5-EF1a-DIO-hChR2(H134R)-mCherry-WPRE-pA. In the hippocampal CA1 region of the injected animals, the expression of mCherry and, accordingly, of ChR2 was targeted to CR-positive interneurons (Fig. 6*A*,*B*). The level of mCherry expression was significantly higher in HO mice (HE mice, 7.2 ± 0.7 cells/slice, $n = 15$; HO mice, 21.3 ± 2.2 cells/slice, $n = 9$; $p < 0.0001$; *t* test), whereas the degree of colocalization of mCherry and CR was similar between the two genotypes (HE animals, 70.1 ± 5.7%, $n = 15$; HO animals, 81.1 ± 4.4%, $n = 9$). Therefore, both HE- and HO-injected mice were used in these experiments. As the population of CR-positive interneurons in the CA1 hippocampus can be heterogeneous, first we performed targeted patch-clamp recordings from infected interneurons and filled them with biocytin to examine their membrane and anatomical properties. Our data showed the presence of at least two distinct subtypes of CR-positive interneurons in the CA1 RAD/PYR. One group of CR-positive cells had a cell body located within the O/A, PYR, or RAD; a multipolar dendritic tree; and a widely projecting axon that mostly occupied the CA1 RAD and PYR (~65%; Fig. 6*C1*). These cells had a high input resistance (482.5 ± 98.2 MΩ; $n = 4$), a small membrane capacitance (52.5 ± 11.3 pF; $n = 4$), and an irregularly spiking or rapidly adapting firing pattern. In several cases ($n = 5$ slices/2 animals), the dendrites of 2–3 CR-positive cells of this subtype were found to form dendro-dendritically connected clusters (Fig. 6*C1*, top inset), which is a hallmark of the type I interneuron-specific (IS1) interneuron described previously in the rat CA1 hippocampus (Gulyás et al., 1996). In addition, we found axosomatic and axodendritic contacts made by CR-positive interneurons onto other CR-positive cells (Fig. 6*C1*, bottom inset). The second subtype of CR-positive interneurons had a soma located within the RAD or PYR, a unipolarly or bipolarly oriented dendritic arbor, and an axon that projected to the O/A (Fig. 6*C2*). Their membrane properties were similar to those of the first type of CR-positive interneurons (input resistance, 512.5 ± 78.3 MΩ; $n = 5$; membrane capacitance, 31.3 ± 2.9 pF; $n = 5$). Therefore, the two cell subtypes could only be distinguished by anatomical properties, with the first subtype likely corresponding to IS1 and the second subtype corresponding to IS3 cells.

To confirm that the second subtype of CR-positive interneurons were indeed IS3 cells, we then examined their connectivity with O/A interneurons using optogenetic circuit mapping. Because ChR2-evoked AP may exhibit distinct properties compared with that evoked by current injection (Schoenenberger et al., 2011), first we performed current-clamp recordings from RAD/PYR interneurons infected with mCherry and ChR2 to compare the properties of APs evoked by blue light (450–490 nm; 5 ms) using wide-field stimulation within the CA1 area (~0.2 mm^2, centered on the stratum oriens; estimated light intensity, 10–20 W/mm^2) with those evoked by somatic current injection (1 nA; 2 ms; Fig. 7*A*). Recorded cells were filled with biocytin and reconstructed and only those that had the anatomical properties of IS3 cells (Fig. 6*C2*) were included in this analysis. We found that light-evoked AP in IS3 cells was almost undistinguishable from that evoked by somatic current injection (Fig. 7*A*), with the exception of the AP after-depolarization (ADP) that was apparent only with light stimulation. We then examined the properties of light-evoked postsynaptic responses in O/A interneurons. Our data showed that light stimulation at −70 mV (using a 50 mM $[Cl^-]_i$ intracellular solution) in the presence of ionotropic glutamate receptor blockers (L-AP5 and NBQX) produced $IPSC_L$s (Fig. 7*B1*) in different types of O/A interneurons ($n = 5$), including OLMs (Fig. 7*B2*), BISs (Fig. 7*B3*), and a putative axo-axonic

cell (Fig. 7*B4*). These responses were blocked by the $GABA_A$ receptor antagonist gabazine (decrease to 3.3 ± 0.9% of control, $n = 3$; Fig. 7*B1*), consistent with their GABAergic nature. Furthermore, in OLM cells, $IPSP_L$s at −40 mV in normal ACSF ($n = 6$) occurred with the same latency as that of light-evoked APs in IS3 cells ($n = 4$; Fig. 7*C*) and were blocked by TTX (1 μM; Fig. 7*D*), suggesting that they were monosynaptic responses generated by sodium spikes initiated in IS3 cells after ChR2 activation. Together, these data indicate that IS3 interneurons are effectively targeted in CR-Cre mice for optical manipulation. Importantly, optical stimulation within the CA1 area produced monosynaptic inhibitory responses in OLM interneurons, which were evoked by sodium spikes in IS3 cells.

IS3 interneurons control the firing rate and timing of OLM cells

To study the impact of IS3 cell activation on the recruitment of OLM cells, next we combined optical stimulation of IS3 cells with current-clamp recordings of OLM interneuron firing. OLM interneurons were depolarized for 2 s to allow their spontaneous firing (V_m, −41.8 ± 3.1 mV; firing rate, 7.3 ± 4.6 Hz; $n = 6$) and wide-field light stimulation was applied to evoke $IPSP_L$s. We found that a single $IPSP_L$ evoked by a pulse of light (5 ms) resulted in a drastic decrease in the firing probability of OLM interneurons (firing probability, 19.6 ± 8.8% of the control; $n = 6$; Fig. 8*A*). Interestingly, after the inhibition period (duration, 33.6 ± 3.3 ms; $n = 6$), the firing of OLM interneurons was increased in three of six interneurons (firing probability, 456.7 ± 192% of the control; Fig. 8*A*), which reflected postinhibitory rebound excitation (Cobb et al., 1995). In these cells, rebound spikes followed by after-hyperpolarizations (seen as a second hyperpolarizing component following $IPSP_L$) were generated with a relatively small jitter (~5.8 ms). The degree of postinhibitory depolarization correlated well with the $IPSP_L$ amplitude and likely reflected the individual variance in the efficiency of ChR2 expression and axon preservation in slices.

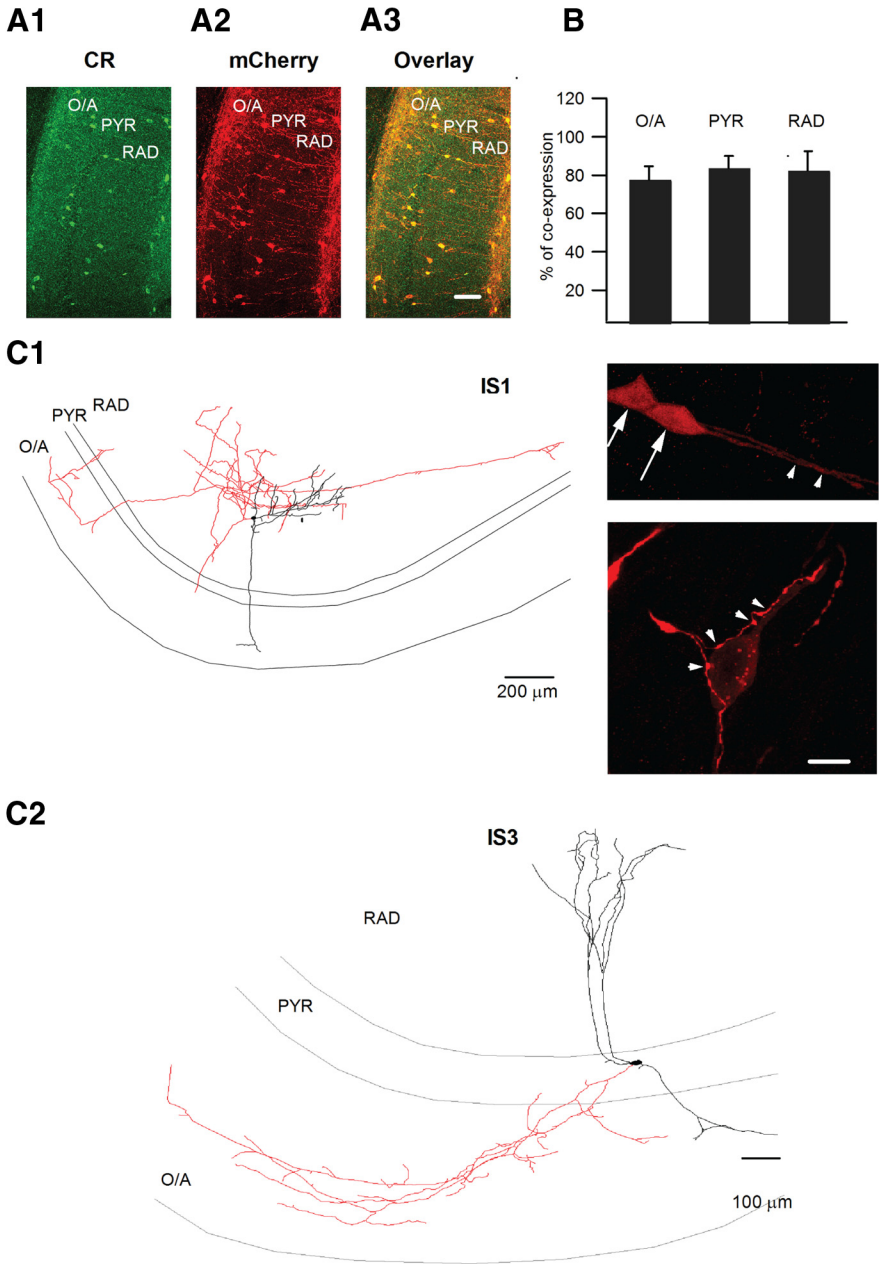

Figure 6. Targeting IS3 cells in CR-Cre mice ***A***, Confocal images showing immunoreactivity for CR (***A1***), mCherry (***A2***), and a superimposition of the two markers (***A3***). Scale bars, 50 μm. ***B***, Summary data illustrating the colocalization of CR and mCherry in different layers of the hippocampal CA1 area of an HO CR-Cre mouse ($n = 9$ slices/two animals). ***C***, Neurolucida reconstructions of two types of CR-positive interneurons targeted with mCherry: putative IS1 (***C1***) and IS3 (***C2***). Top inset shows CR-positive interneurons making dendro-dendritic contacts (with arrows indicating the cell bodies and arrowheads highlighting the dendro-dendritic contacts); lower inset shows axosomatic and axodendritic contacts made on CR-positive interneuron by CR-positive terminals. Scale bar, 10 μm.

It should be noted that the light-evoked AP in IS3 cells was followed by a large ADP (Fig. 7*A*) that could result in enhanced GABA release at IS3–OLM synapses in optogenetic experiments. To explore this issue, we recorded $IPSC_L$s evoked by single-cell laser stimulation in OLM interneurons (which were identified anatomically *post hoc*) and compared their properties with those of uIPSCs obtained in paired recordings in slices from VIP-eGFP mice. Voltage-clamp recordings from OLM interneurons were obtained at 0 mV using a Cs^+-based intracellular solution (conditions similar to paired recordings in slices from VIP-eGFP mice) and putative IS3 cells were identified based on their morphological features. In the case of synaptic connection, focusing the laser beam (488 nm) at the level of the IS3 soma (diameter, 10–15 μm) resulted in $IPSC_L$s in OLM cells. The laser intensity was then adjusted to obtain successes and failures of $IPSC_L$s similar to that seen in paired recordings (Schoenenberger et al., 2011). The $IPSC_L$s obtained under these conditions were considered as unitary and their properties were analyzed. Importantly, despite the presence of the larger-amplitude ADPs in light-evoked spikes, the unitary $IPSC_L$s evoked by single-cell laser stimulation were indistinguishable from those obtained in paired

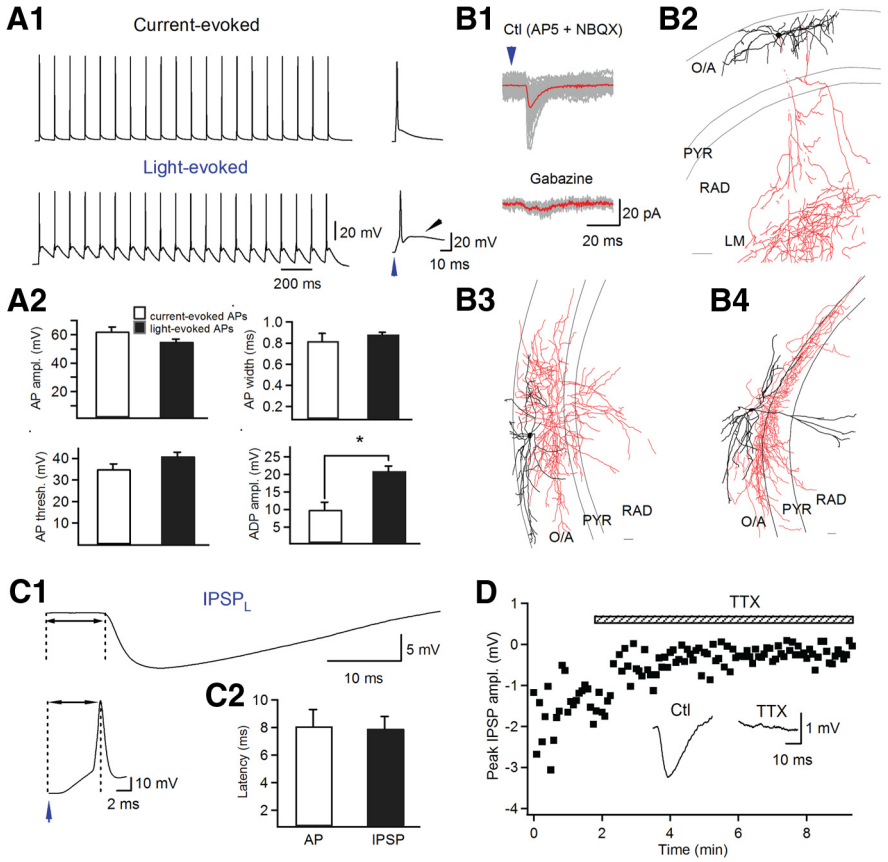

Figure 7. ChR2-based mapping of IS3 interneuron targets ***A***, Comparison of the properties of the APs evoked by somatic current injection versus those evoked by ChR2-based photostimulation. ***A1***, Representative examples of the trains of APs evoked by somatic current injection (1 nA, 2 ms, 10 Hz; top) and by stimulation with light (5 ms, 10 Hz; bottom). The traces shown at right are individual APs expanded. The blue arrowhead indicates the period at which the pulse of light was applied. The black arrowhead points to the ADP observed in light-evoked responses. ***A2***, Summary data showing the AP amplitude, half-width, and threshold and the ADP amplitude for the current- and light-evoked APs. ***B***, Representative examples of IPSC$_L$s evoked in control (in ACSF containing AP5 and NBQX) and in the presence of gabazine (***B1***) in different subtypes of O/A interneurons, including OLMs (***B2***), BISs (***B3***), and a putative axo-axonic cell (***B4***). Scale bars, 100 μm. ***C***, Representative examples (***C1***) and summary bar graph (***C2***) illustrating the latency of the light-evoked APs and IPSP$_L$s. ***D***, Sample traces and summary plot showing the effect of TTX on the IPSP$_L$s. Note that IPSP$_L$s were blocked by TTX.

recordings (uIPSC$_L$ failure rate: 58.7 ± 5.2%; potency: 21.2 ± 4.0 pA; rise time: 1.7 ± 0.4 ms; decay time constant: 9.2 ± 3.0 ms; n = 3; Fig. 8*B*), indicating that the light-evoked silencing of OLM interneurons was physiological in nature.

If a single AP generated synchronously in several IS3 cells is able to control the firing rate and timing of individual OLM interneurons, what is the impact of a repetitive firing of IS3 cells on the activity of OLMs? We found that the application of a train of light pulses at 5 or 10 Hz for 1 s during weak irregular firing of OLM cells was sufficient to pace their activity (Fig. 8*C2*,*C3*). Consistent with previous reports on the intrinsic theta oscillations and characteristic resonance behavior of OLM interneurons at theta frequency (Gillies et al., 2002; Zemankovics et al., 2010), the lower (1 Hz) or higher (20 Hz) frequency of light stimulation were still efficient in silencing OLMs but had a lower impact on their rhythmic activity (Fig. 8*C1*,*C4*). Because repetitive activity at IS3-OLM synapses may affect the firing probability of OLMs through the induction of short-term synaptic plasticity (Chamberland et al., 2010), we examined changes in IPSP$_L$ amplitude during different frequencies of light stimulation, but found no significant differences at all frequencies tested (n = 6; $p > 0.05$; paired t test; Fig. 8*D*). Consistent with these findings, the amplitude of the uIPSCs obtained in paired recordings at IS3–OLM synapses in slices from VIP-eGFP mice remained unchanged at all frequencies of firing of IS3 cells (Fig. 4*C*). Together, these results indicate that the dendritic inhibition provided by IS3 cells is able to coordinate the firing rate and timing of OLM interneurons and pace their activity at a theta frequency when several IS3 cells fire at the same time.

Discussion

In this study, we investigated the properties of the inhibition originating from a subtype of hippocampal IS interneurons and the manner in which this local inhibitory input may regulate the output of the CA1 feedback inhibitory circuitry. Consistent with earlier anatomical findings, our data revealed that IS3 cells make inhibitory synapses onto several O/A interneurons, including OLMs, BISs, BCs, and oriens–oriens interneurons. OLM dendrites were the preferential target of IS3 cells. Accordingly, the uIPSCs evoked at IS3–OLM synapses had a small amplitude and slow kinetics. Furthermore, an IS3 cell contacted an OLM via multiple release sites with a low release probability. Finally, inhibition provided by IS3 interneurons was able to regulate the firing rate and timing of OLM cells, indicating that dendritic inhibition in OLM interneurons controls their recruitment during network activity.

Identification and functional connectivity of IS3 cells

For over a decade since their discovery, hippocampal IS cells remained unstudied in terms of their physiological organization and function. Using a combination of anatomical, electrophysiological, and neurochemical criteria in specific mouse models, we were able to target these cells for detailed functional characterization. In agreement with a general consensus on interneuron classification (DeFelipe et al., 2013), our data showed that a single set of criteria (e.g., membrane properties or expression of markers) is insufficient to discriminate these cells from other types of GABAergic interneurons. In fact, similar to other interneuron types, IS cells showed a high input resistance, a small membrane capacitance, and an irregularly spiking firing pattern. Moreover, although IS3 cells can be distinguished based on the coexpression of VIP and CR, VIP and CR alone are expressed by several distinct types of hippocampal interneurons (Lorén et al., 1979; Köhler, 1982; Léránth et al., 1984; Miettinen et al., 1992; Tricoire et al., 2011) and detailed anatomical and functional analyses of the cells targeted in different mouse models (VIP-eGFP and CR-Cre) were crucial for the identification of IS3 cells.

In terms of anatomical properties, IS3 cells in the mouse hippocampus were similar to those described originally in the rat hippocampus. These cells innervated heavily the O/A border, although occasional axonal branches were found in the RAD and

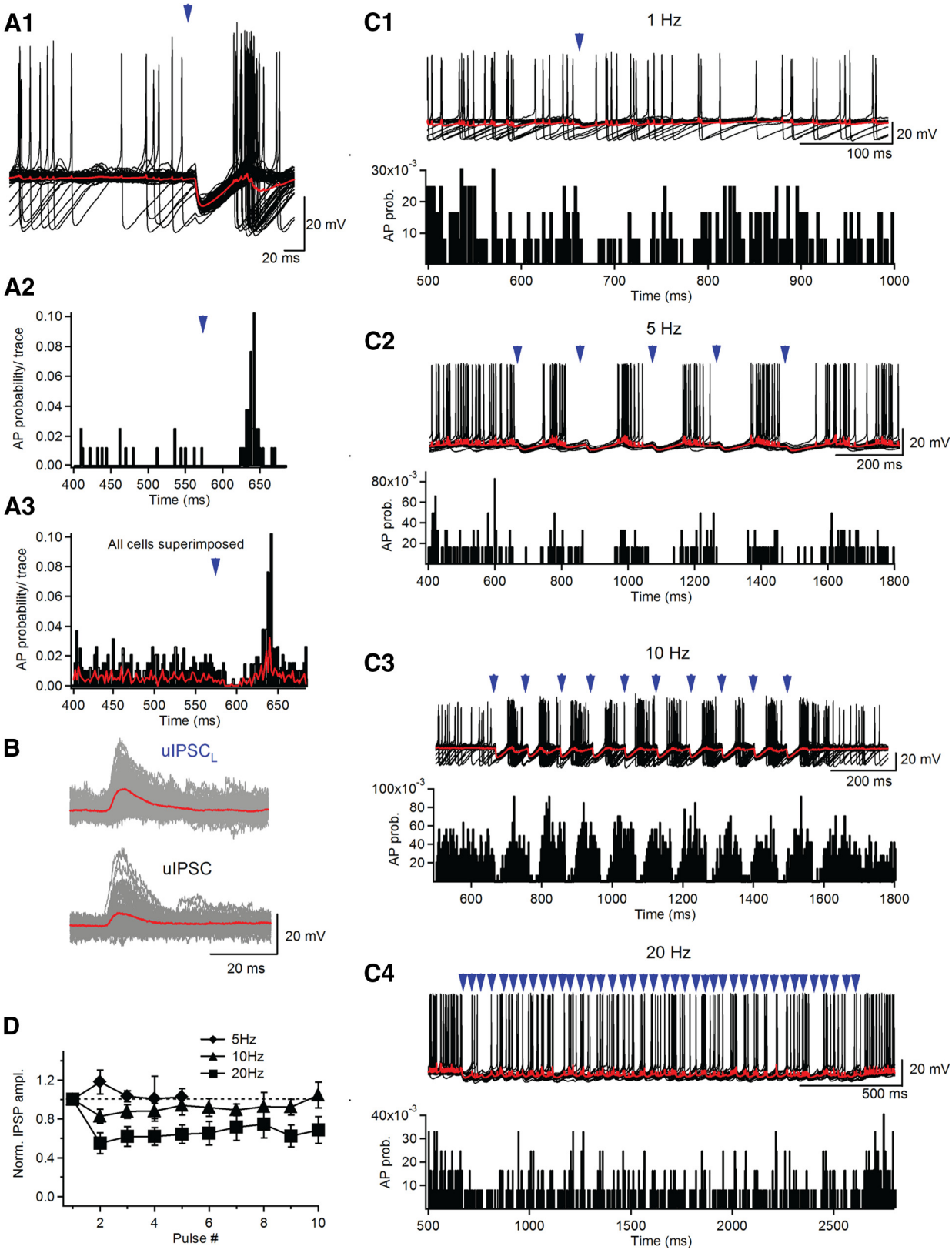

Figure 8. IS3 cells control the firing rate and timing of OLM cells ***A***, Effect of light stimulation on OLM interneuron firing. ***A1***, Representative example of a current-clamp recording obtained from an OLM interneuron before, during, and after light stimulation. Individual traces are shown in black and the average is shown in red. The blue arrowhead indicates the period of time at which the light pulse was applied. ***A2***, ***A3***, Cumulative histograms of the AP probability for the example illustrated in ***A1*** (***A2***) and for all cells recorded in these experiments (***A3***; $n = 6$). The average spike probability is shown in red. ***B***, Comparison of uIPSC$_L$s (top) and by a single presynaptic AP during paired recordings (uIPSC, bottom). ***C***, Firing of OLMs during 1, 5, 10, and 20 Hz light stimulation. ***C1***–***C4***, Representative examples of current-clamp recordings and average cumulative histograms of the AP probability obtained from OLM interneurons before, during, and after light stimulation at 1 Hz (***C1***), 5 Hz (***C2***), 10 Hz (***C3***), and 20 Hz (***C4***). Individual traces are shown in black and the average is shown in red. The blue arrowheads point to the periods at which the light pulses were applied. ***D***, Summary plot showing an absence of significant changes in the amplitude of IPSP$_L$s during 5, 10, and 20 Hz light stimulation ($p > 0.05$; ANOVA; $n = 6$).

PYR. Their dendritic arbors were often unipolar (47% of cells), suggesting that these cells are preferentially recruited through the activation of the Schaffer collaterals, the temporoammonic pathway, and, likely, thalamic excitatory projections. However, the mechanisms underlying the input-specific recruitment of IS3 cells during network activity remain to be determined.

In agreement with a previous ultrastructural analysis of IS3 cell targets in the rat hippocampus (Acsády et al., 1996b; Gulyás et al., 1996), we found no evidence of synaptic connection between IS3 cells and PCs in the murine hippocampus. Furthermore, the results of our functional experiments showed that although OLM interneurons were the preferential target of IS3 cells, other dendritic and perisomatic sources of inhibition to PCs are controlled by the IS3 circuitry. In fact, the connectivity ratio of IS3 interneurons was quite high, because almost every third pair of interneurons tested was connected. Furthermore, in all cases, IS3 cells provided dendritic inhibition to their targets. Accordingly, the uIPSCs evoked at different targets were similarly small and slow, with the exception of BISs. In these cells, uIPSCs had much faster kinetics. Importantly, the potency of uIPSCs at IS3–BIS synapses was similar to that observed at IS3–OLM synapses, thus arguing against the target-specific dendritic location of IS3 synapses in these two cells. Alternatively, the target-specific composition of $GABA_A$ receptor subunits may explain such differences in uIPSC kinetics. Similar to findings obtained in PCs, inhibitory synapses onto interneurons may be composed of different $GABA_A$ receptor subunits (Hájos and Mody, 1997; Patenaude et al., 2001; Salesse et al., 2011). In particular, synaptic expression of the α5 $GABA_A$ receptor subunit ($GABA_A$-α5), which is responsible for kinetically slow IPSCs, has been reported in the CA1 hippocampus and in OLM interneurons (Loebrich et al., 2006; Prenosil et al., 2006; Ali and Thomson, 2008; Zarnowska et al., 2009; Salesse et al., 2011). The latter may explain a slower time course of uIPSCs in OLMs compared with BISs. However, the input- and target-specific synaptic expression of the $GABA_A$-α5 is currently unknown.

Using the CR-Cre mouse model, we were able to examine other types of CR-positive interneurons located in the RAD and PYR of the CA1 hippocampus and thus target putative type I IS cells (Gulyás et al., 1996). This subtype of IS cells exhibited a remarkable anatomical diversity, with cell bodies that occupied different layers and an axon that projected mostly within the RAD and PYR. Similar to IS3 cells, IS1 cells exhibited a high input resistance but were more heterogeneous in terms of firing properties. Therefore, more than one subtype of putative IS1 cells is likely to be found within this group of CR-positive interneurons. Paired recordings and detailed analysis of the anatomical and physiological features of these cells, as well as of their postsynaptic targets, will be required to address this question.

Unitary conductance at IS3–OLM synapses and OLM recruitment

Our data indicate that the uIPSCs evoked in OLM interneurons by the activation of IS3 cells had small amplitude and high failure rate. Furthermore, the amplitude of uIPSCs at IS3–OLM synapses remained low during theta- or β-like activity (10–20 Hz) and was only increased during the high-frequency firing (100 Hz) of IS3 cells due to efficient summation of uIPSCs. These data indicate that the random recruitment of single IS3 cells will only have an impact when they fire at high frequencies. However, despite the low efficiency of transmission at single IS3 synapses, many IS3 cells appear to converge onto a single OLM interneuron. Given the total number of IS3 axonal boutons that innervate the O/A in a 300 μm slice (~70) and multiple synaptic contacts made by a single IS3 onto an OLM, we can estimate that an IS3 cell is likely to contact nearly all OLM interneurons residing in its zone of innervation. Accordingly, a single OLM may receive inputs from virtually all IS3 interneurons in this area (6–7 cells). Therefore, the synchronous activation of 6–7 IS3 cells may be needed for the efficient control of the OLM output in the case of low-frequency firing of IS3 interneurons. In this context, the IS3–OLM circuitry is likely built to operate in two distinct modes: weak inhibition or even disinhibition of OLMs during sparse hippocampal activity and efficient inhibition during high-frequency network oscillations and synchronous activation of a number of IS3 cells.

Functional significance of IS3 inhibition for CA1 circuitry

We showed that dendritic inhibition originating from the IS3 circuitry is able to regulate the AP output of OLM interneurons. Similar to those observed in PCs (Müller et al., 2012), these data may have important implications for excitatory–inhibitory interactions in the dendrites of OLM cells, which receive predominantly local excitatory input from the CA1 PCs and exhibit a particularly high density of voltage-gated Na^+ channels playing an important role in initiation of dendritic Na^+ spikes (Blasco-Ibáñez and Freund, 1995; Martina et al., 2000; Takács et al., 2012). Although the mechanisms underlying the interactions between different inputs in OLM dendrites remain to be elucidated, it is clear that dense inhibitory innervation by IS3 cells may control dendritic spike initiation. By silencing OLM interneurons and probably other dendrite-targeting O/A interneurons (such as BIS and oriens–oriens interneurons), IS3 cells may be involved in the regulation of dendritic electrogenesis, gating, and burst firing in PCs (Lovett-Barron et al., 2012; Royer et al., 2012). The limited datasets available regarding the role of IS3 cells in the recruitment of other anatomically identified O/A interneurons did not allow us to determine whether the output of different subtypes of interneurons is similarly controlled by the IS3 circuitry. However, it is expected that high-frequency firing of IS3 clusters during network oscillations will have a significant impact on the recruitment of several distinct subtypes of O/A interneurons, thus controlling the rate, burst, and timing of hippocampal PCs. These functions of the IS3 circuitry will depend on the target-specific differences in the properties of IS3 synapses. Under which conditions might this happen? Unfortunately, the *in vivo* firing patterns of IS interneurons during different network states remain unknown. Given that OLM cells may be silenced during sharp wave ripples (SWRs) *in vivo* (Klausberger et al., 2003; Varga et al., 2012), we can suggest that large populations of IS3 cells can be recruited during SWRs and suppress OLM activity. The particularly high input resistance of IS interneurons point to their high excitability. However, so far, these cells have not been identified among the active interneuronal populations in anesthetized animals (P. Somogyi, personal communication), suggesting that anesthesia may hamper their recruitment. Further experiments on drug-free animals followed by unambiguous anatomical identification (Lapray et al., 2012; Varga et al., 2012) will be required to determine the activity-dependent recruitment of IS cells *in vivo* and their role in CA1 hippocampal computations.

References

Acsády L, Arabadzisz D, Freund TF (1996a) Correlated morphological and neurochemical features identify different subsets of vasoactive intestinal polypeptide-immunoreactive interneurons in rat hippocampus. Neuroscience 73:299–315. CrossRef Medline

Acsády L, Görcs TJ, Freund TF (1996b) Different populations of vasoactive intestinal polypeptide-immunoreactive interneurons are specialized to control pyramidal cells or interneurons in the hippocampus. Neuroscience 73:317–334. CrossRef Medline

Ali AB, Thomson AM (2008) Synaptic alpha 5 subunit-containing GABAA receptors mediate IPSPs elicited by dendrite-preferring cells in rat neocortex. Cereb Cortex 18:1260–1271. CrossRef Medline

Blasco-Ibáñez JM, Freund TF (1995) Synaptic input of horizontal interneurons in stratum oriens of the hippocampal CA1 subfield: structural basis of feed-back activation. Eur J Neurosci 7:2170–2180. CrossRef Medline

Chamberland S, Topolnik L (2012) Inhibitory control of hippocampal inhibitory neurons. Front Neurosci 6:165. CrossRef Medline

Chamberland S, Salesse C, Topolnik D, Topolnik L (2010) Synapse-specific inhibitory control of hippocampal feedback inhibitory circuit. Front Cell Neurosci 4:130. CrossRef Medline

Clements JD, Silver RA (2000) Unveiling synaptic plasticity: a new graphical and analytical approach. Trends Neurosci 23:105–113. CrossRef Medline

Cobb SR, Buhl EH, Halasy K, Paulsen O, Somogyi P (1995) Synchronization of neuronal activity in hippocampus by individual GABAergic interneurons. Nature 378:75–78. CrossRef Medline

Daw MI, Tricoire L, Erdelyi F, Szabo G, McBain CJ (2009) Asynchronous transmitter release from cholecystokinin-containing inhibitory interneurons is widespread and target-cell independent. J Neurosci 29:11112–11122. CrossRef Medline

DeFelipe J, López-Cruz PL, Benavides-Piccione R, Bielza C, Larrañaga P, Anderson S, Burkhalter A, Cauli B, Fairén A, Feldmeyer D, Fishell G, Fitzpatrick D, Freund TF, González-Burgos G, Hestrin S, Hill S, Hof PR, Huang J, Jones EG, Kawaguchi Y, et al. (2013) New insights into the classification and nomenclature of cortical GABAergic interneurons. Nat Rev Neurosci 14:202–216. CrossRef Medline

Ferraguti F, Cobden P, Pollard M, Cope D, Shigemoto R, Watanabe M, Somogyi P (2004) Immunolocalization of metabotropic glutamate receptor 1alpha (mGluR1alpha) in distinct classes of interneuron in the CA1 region of the rat hippocampus. Hippocampus 14:193–215. CrossRef Medline

Földy C, Lee SH, Morgan RJ, Soltesz I (2010) Regulation of fast-spiking basket cell synapses by the chloride channel ClC-2. Nat Neurosci 13:1047–1049. CrossRef Medline

Gillies MJ, Traub RD, LeBeau FE, Davies CH, Gloveli T, Buhl EH, Whittington MA (2002) A model of atropine-resistant theta oscillations in rat hippocampal area CA1. J Physiol 543:779–793. CrossRef Medline

Gillis KD (1995) Techniques for membrane capacitance measurements. In: Single channel recording, Ed 2 (Sakmann B, Neher E), 155–198. New York: Plenum.

Glickfeld LL, Scanziani M (2006) Distinct timing in the activity of cannabinoid-sensitive and cannabinoid-insensitive basket cells. Nat Neurosci 9:807–815. CrossRef Medline

Gulyás AI, Hájos N, Freund TF (1996) Interneurons containing calretinin are specialized to control other interneurons in the rat hippocampus. J Neurosci 16:3397–3411. Medline

Hájos N, Mody I (1997) Synaptic communication among hippocampal interneurons: properties of spontaneous IPSCs in morphologically identified cells. J Neurosci 17:8427–8442. Medline

Hefft S, Jonas P (2005) Asynchronous GABA release generates long-lasting inhibition at a hippocampal interneuron-principal neuron synapse. Nat Neurosci 8:1319–1328. CrossRef Medline

Klausberger T, Somogyi P (2008) Neuronal diversity and temporal dynamics: the unity of hippocampal circuit operations. Science 321:53–57. CrossRef Medline

Klausberger T, Magill PJ, Márton LF, Roberts JD, Cobden PM, Buzsáki G, Somogyi P (2003) Brain-state- and cell-type-specific firing of hippocampal interneurons in vivo. Nature 421:844–848. CrossRef Medline

Klausberger T, Márton LF, Baude A, Roberts JD, Magill PJ, Somogyi P (2004) Spike timing of dendrite-targeting bistratified cells during hippocampal network oscillations in vivo. Nat Neurosci 7:41–47. CrossRef Medline

Klausberger T, Márton LF, O'Neill J, Huck JH, Dalezios Y, Fuentealba P, Suen WY, Papp E, Kaneko T, Watanabe M, Csicsvari J, Somogyi P (2005) Complementary roles of cholecystokinin- and parvalbumin-expressing GABAergic neurons in hippocampal network oscillations. J Neurosci 25:9782–9793. CrossRef Medline

Köhler C (1982) Distribution and morphology of vasoactive intestinal polypeptide-like immunoreactive neurons in regio superior of the rat hippocampal formation. Neurosci Lett 33:265–270. CrossRef Medline

Kosaka T, Kosaka K, Tateishi K, Hamaoka Y, Yanaihara N, Wu JY, Hama K (1985) GABAergic neurons containing CCK-8-like and/or VIP-like immunoreactivities in the rat hippocampus and dentate gyrus. J Comp Neurol 239:420–430. CrossRef Medline

Lapray D, Lasztoczi B, Lagler M, Viney TJ, Katona L, Valenti O, Hartwich K, Borhegyi Z, Somogyi P, Klausberger T (2012) Behavior-dependent specialization of identified hippocampal interneurons. Nat Neurosci 15:1265–1271. CrossRef Medline

Lawrence JJ, Grinspan ZM, McBain CJ (2004) Quantal transmission at mossy fibre targets in the CA3 region of the rat hippocampus. J Physiol 554:175–193. CrossRef Medline

Léránth C, Frotscher M, Tömböl T, Palkovits M (1984) Ultrastructure and synaptic connections of vasoactive intestinal polypeptide-like immunoreactive non-pyramidal neurons and axon terminals in the rat hippocampus. Neuroscience 12:531–542. CrossRef Medline

Loebrich S, Bähring R, Katsuno T, Tsukita S, Kneussel M (2006) Activated radixin is essential for GABAA receptor alpha5 subunit anchoring at the actin cytoskeleton. EMBO J 25:987–999. CrossRef Medline

Lorén I, Emson PC, Fahrenkrug J, Björklund A, Alumets J, Håkanson R, Sundler F (1979) Distribution of vasoactive intestinal polypeptide in the rat and mouse brain. Neuroscience 4:1953–1976. CrossRef Medline

Lovett-Barron M, Turi GF, Kaifosh P, Lee PH, Bolze F, Sun XH, Nicoud JF, Zemelman BV, Sternson SM, Losonczy A (2012) Regulation of neuronal input transformations by tunable dendritic inhibition. Nat Neurosci 15:423–430, S1–S3. CrossRef Medline

Martina M, Vida I, Jonas P (2000) Distal initiation and active propagation of action potentials in interneuron dendrites. Science 287:295–300. CrossRef Medline

Maurer AP, Cowen SL, Burke SN, Barnes CA, McNaughton BL (2006) Phase precession in hippocampal interneurons showing strong functional coupling to individual pyramidal cells. J Neurosci 26:13485–13492. CrossRef Medline

Miettinen R, Gulyás AI, Baimbridge KG, Jacobowitz DM, Freund TF (1992) Calretinin is present in non-pyramidal cells of the rat hippocampus. II. Co-existence with other calcium binding proteins and GABA. Neuroscience 48:29–43. CrossRef Medline

Milner B (1972) Disorders of learning and memory after temporal lobe lesions in man. Clin Neurosurg 19:421–446. Medline

Müller C, Beck H, Coulter D, Remy S (2012) Inhibitory control of linear and supralinear dendritic excitation in CA1 pyramidal neurons. Neuron 75:851–864. CrossRef Medline

Nitz D, McNaughton B (2004) Differential modulation of CA1 and dentate gyrus interneurons during exploration of novel environments. J Neurophysiol 91:863–872. Medline

Pangalos M, Donoso JR, Winterer J, Zivkovic AR, Kempter R, Maier N, Schmitz D (2013) Recruitment of oriens-lacunosum-moleculare interneurons during hippocampal ripples. Proc Natl Acad Sci U S A 110:4398–4403. CrossRef Medline

Patenaude C, Nurse S, Lacaille JC (2001) Sensitivity of synaptic GABA(A) receptors to allosteric modulators in hippocampal oriens-alveus interneurons. Synapse 41:29–39. CrossRef Medline

Pitler TA, Alger BE (1992) Postsynaptic spike firing reduces synaptic GABAA responses in hippocampal pyramidal cells. J Neurosci 12:4122–4132. Medline

Prenosil GA, Schneider Gasser EM, Rudolph U, Keist R, Fritschy JM, Vogt KE (2006) Specific subtypes of GABAA receptors mediate phasic and tonic forms of inhibition in hippocampal pyramidal neurons. J Neurophysiol 96:846–857. CrossRef Medline

Royer S, Zemelman BV, Losonczy A, Kim J, Chance F, Magee JC, Buzsáki G (2012) Control of timing, rate and bursts of hippocampal place cells by dendritic and somatic inhibition. Nat Neurosci 15:769–775. CrossRef Medline

Salesse C, Mueller CL, Chamberland S, Topolnik L (2011) Age-dependent remodelling of inhibitory synapses onto hippocampal CA1 oriens-lacunosum moleculare interneurons. J Physiol 589:4885–4901. CrossRef Medline

Schoenenberger P, Schärer YP, Oertner TG (2011) Channelrhodopsin as a tool to investigate synaptic transmission and plasticity. Exp Physiol 96:34–39. CrossRef Medline

Sloviter RS, Nilaver G (1987) Immunocytochemical localization of GABA-, cholecystokinin-, vasoactive intestinal polypeptide-, and somatostatin-like immunoreactivity in the area dentata and hippocampus of the rat. J Comp Neurol 256:42–60. CrossRef Medline

Takács VT, Klausberger T, Somogyi P, Freund TF, Gulyás AI (2012) Extrinsic and local glutamatergic inputs of the rat hippocampal CA1 area differentially innervate pyramidal cells and interneurons. Hippocampus 22: 1379–1391. CrossRef Medline

Tricoire L, Pelkey KA, Daw MI, Sousa VH, Miyoshi G, Jeffries B, Cauli B, Fishell G, McBain CJ (2010) Common origins of hippocampal Ivy and nitric oxide synthase expressing neurogliaform cells. J Neurosci 30:2165–2176. CrossRef Medline

Tricoire L, Pelkey KA, Erkkila BE, Jeffries BW, Yuan X, McBain CJ (2011) A blueprint for the spatiotemporal origins of mouse hippocampal interneuron diversity. J Neurosci 31:10948–10970. CrossRef Medline

Tukker JJ, Fuentealba P, Hartwich K, Somogyi P, Klausberger T (2007) Cell type-specific tuning of hippocampal interneuron firing during gamma oscillations in vivo. J Neurosci 27:8184–8189. CrossRef Medline

Varga C, Golshani P, Soltesz I (2012) Frequency-invariant temporal ordering of interneuronal discharges during hippocampal oscillations in awake mice. Proc Natl Acad Sci U S A 109:E2726–E2734. CrossRef Medline

Vincent P, Armstrong CM, Marty A (1992) Inhibitory synaptic currents in rat cerebellar Purkinje cells: modulation by postsynaptic depolarization. J Physiol 456:453–471. Medline

Zarnowska ED, Keist R, Rudolph U, Pearce RA (2009) GABAA receptor alpha5 subunits contribute to GABAA, slow synaptic inhibition in mouse hippocampus. J Neurophysiol 101:1179–1191. CrossRef Medline

Zemankovics R, Káli S, Paulsen O, Freund TF, Hájos N (2010) Differences in subthreshold resonance of hippocampal pyramidal cells and interneurons: the role of h-current and passive membrane characteristics. J Physiol 588:2109–2132. CrossRef Medline